

Simulate response of RC columns under cyclic loads by OpenSees platform

Mô phỏng ứng xử của cột bê tông cốt thép chịu tải trọng lặp bằng phần mềm OpenSees

Pham Phu Anh Huy^{a,b*}
Phạm Phú Anh Huy^{a,b*}

^aInstitute of Research and Development, Duy Tan University, Da Nang, 550000, Vietnam

^aViện Nghiên cứu và Phát triển Công nghệ cao, Trường Đại học Duy Tân, Đà Nẵng, Việt Nam

^bFaculty of Civil Engineering, Duy Tan University, Da Nang, 550000, Vietnam

^bKhoa Xây dựng, Trường Đại học Duy Tân, Đà Nẵng, Việt Nam

(Date of receiving article: 16/11/2023, date of completion of review: 28/02/2024, date of acceptance for posting: 06/03/2024)

Abstract

Hysteresis loops play a pivotal role in assessing the behavior of reinforced concrete (RC) columns, particularly when subjected to cyclic loads or seismic events. This article aims to elucidate the significance of employing hysteresis curves for the analysis of RC column behavior. In addition, the paper introduced a novel model designed to construct hysteresis curves for RC columns featuring rectangular cross-sections. This innovative model is implemented within the OpenSees platform comprising three springs that simulate the degradation of shear and stiffness. To verify its accuracy, the model's outcomes are rigorously compared against experimental data. The results unequivocally demonstrate that the three-spring model adeptly replicates the hysteresis loops of RC columns, with an average tolerance approaching unity, highlighting its exceptional accuracy and potential utility.

Keywords: hysteresis loop; seismic response; cyclic response; RC column; OpenSees.

Tóm tắt

Đường cong trễ là một đồ thị đóng một vai trò quan trọng trong việc đánh giá ứng xử của cột bê tông cốt thép (BTCT), đặc biệt khi chúng phải chịu tải trọng lặp hoặc động đất. Mục tiêu của bài báo là làm rõ tầm quan trọng của việc sử dụng đường cong trễ để phân tích hành vi của các cột RC. Hơn nữa, bài báo giới thiệu một mô hình mới được đề xuất để xây dựng đường cong trễ cho cột BTCT có tiết diện hình chữ nhật. Mô hình đề xuất này được xây dựng dựa trên phần mềm OpenSees với ba liên kết lò xo để mô phỏng sự giảm cường độ, độ cứng. Để xác thực độ chính xác của mô hình đề xuất, các kết quả của mô hình được so sánh với các dữ liệu thực nghiệm. Kết quả so sánh cho thấy rằng mô hình ba lò xo đã mô phỏng một cách khá chính xác vòng lặp trễ của các cột BTCT, với sai số trung bình gần đến một, cho thấy độ chính xác rất tốt và khả năng áp dụng của nó.

Từ khóa: vòng lặp trễ; ứng xử động đất; ứng xử lặp; cột BTCT OpenSees.

*Corresponding author: Pham Phu Anh Huy

Email: phampanhhuy@duytan.edu.vn

1. Introduction

The load-displacement curve for cyclic reversal load or displacement could be called the hysteresis loop. The hysteresis loop expresses in terms of inelastic restoring force-translational displacement relationship. It is a crucial parameter for the seismic inelastic evaluation of RC columns [1–5]. Numerous hysteresis models have been developed to simulate the response of RC columns. For instance, Clough [6] was a researcher among early researchers who investigated the effect of stiffness degradation in RC structural members on the inelastic response of multistory buildings to earthquakes. Inelastic dynamic responses of two idealized multistory buildings are analyzed for ordinary bilinear hysteresis behavior and bilinear hysteresis behavior with stiffness degradation property. However, Clough [6] found that it was not able to predict the maximum response of a stiffness deterioration from results for the corresponding ordinary bilinear system. Takeda et al. [7] conducted a series of RC specimens that were subjected to static tests and periodic earthquake motions. An analytical model was developed to simulate the earthquake response of the elements and materials involved. Takeda et al. [7] proposed a hysteresis loop that were defined by the proposed force-displacement relationship. It was not necessary to invoke additional sources of energy dissipation for a satisfactory prediction of the dynamic response. Takeda et al.

[7] also proposed three linear segments for the displacement-load curve. The first segment in the curve refers to cracking point (P_{cr}, D_{cr}) that were computed with concrete flexure tensile strength. The yield load P_y was obtained by assuming a parabolic compressive stress-strain curve for the concrete. The yield deflection (D_y) was the sum of four parts such as (1) the flexural deflection caused by curvature based on a cracked section; (2) the slip deflection caused by the slip of the longitudinal reinforcement and depression of the concrete at the beam-column interface; (3) the deflection caused by deformation of the platform; and (4) the shear deflection. The hysteresis loop was proposed as presented in Figure 1. Ozcebe et al. [8] proposed a hysteresis shear model for the shear response of RC members subjected to shear force and bending moment reversals as presented in Figure 2. The model consists of a primary shear backbone curve, unloading and reloading branches under cyclic loading. The primary curve is defined by any suitable procedure, i.e., using the fiber section method, or using compression field theory is acceptable. However, these procedures had to have a definition of cracking and yield points. The authors considered the interaction between flexure, shear, and axial force under monotonic loading. Furthermore, the confinement of concrete core and strain hardening of reinforcing steel was also accounted for.

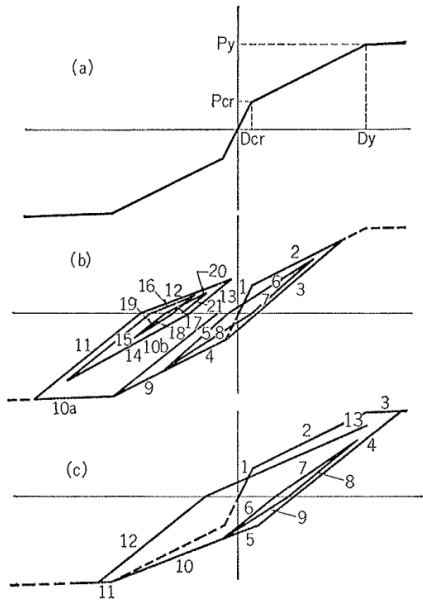


Figure 1. Load-deformation curve (Takeda et al. [7])

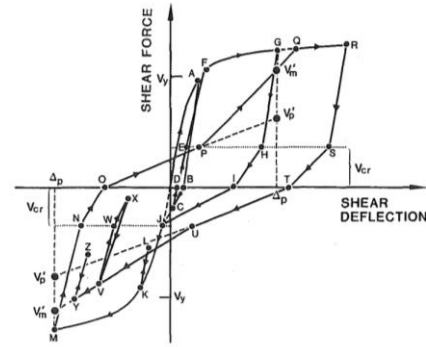


Figure 2. Hysteresis rules (Ozcebe et al. [8])

In addition, Lowes et al. [9] proposed a model to simulate the response of RC beam-column joints under reversed cyclic loading. The model consists of a quad-linear backbone and deterioration of strength and stiffness. This deterioration was based on the energy and displacement rules. The simple process was proposed to analyze the primary inelastic mechanism that simulated the failure of the joint core under shear load and anchorage failure of longitudinal steel embedded in the joint.

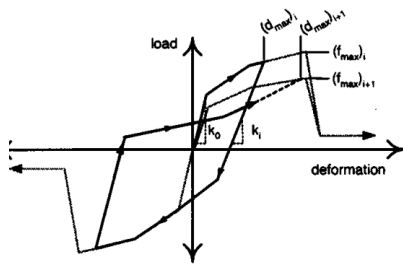


Figure 3. Hysteresis rules (Lowes et al. [9])

Lignos et al. [11] built a backbone curve that presented the relationship between moment and rotation angle as presented in Figure 5. The backbone curve was defined by three parameters (such as effective yield moment M_y , capping moment strength M_c or post-yield strength ratio M_c/M_y , residual moment $M_r = \kappa M_c$), and four

Sezen et al. [10] implemented the hysteresis loop of RC columns by summation of separate three components, i.e., flexure, shear, and slip hysteresis models. The hysteresis rules for flexure and slip components were the same and presented in Figure 4 with slope factors $k_0, k_1, k_2,$ and k_3 . The flexure hysteresis model was based on the model of Takeda et al. [7] with the modification. These changes were conducted by comparison with experimental results.

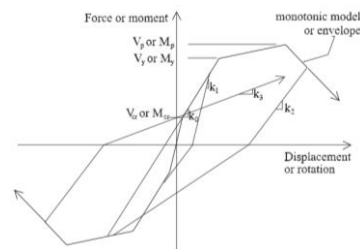


Figure 4. Hysteresis rules (Sezen et al. [10])

deformation parameters (yield rotation θ_y , pre-capping plastic rotation θ_p , post-capping plastic rotation θ_{pc} , ultimate rotation capacity θ_u). Yet, Lignos et al. [11] implemented hysteresis rules that simulate the effect of the cyclic moment-rotation relationship at plastic hinge regions in beams.

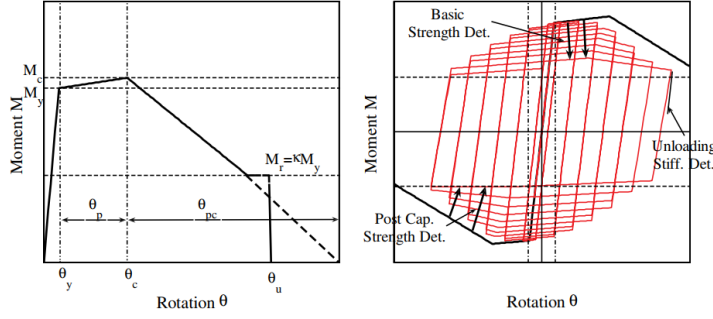


Figure 5. Monotonic and hysteresis rules (Lignos et al. [11])

Lee et al. [12] accurately and efficiently simulated the cyclic behavior of old RC columns by using the Pinching4 model that considered pinching and cyclic deterioration. It can be seen that the Pinching4 material model with the proposed empirical equations accurately simulated the cyclic behavior of both flexure-shear and shear-critical columns, including pinching and cyclic degradation in strength and stiffness. They proposed the monotonic backbone curve and cyclic deterioration and pinching, as presented in Figure 6. Modeling

parameters were implemented based on the forty flexure-shear and shear critical column tests. The pinching4 model can represent a pinched load-deformation response of the members that exhibited cyclic degradation in strength and stiffness. Three parameters $rDisp$, $rForce$, $Uforce$ control pinching behavior. $rDisp$, $rForce$ will control pinching behavior in the reloading branch. $Uforce$ controls the degree of pinching. Lee et al. [12] proposed the equations that predicted three parameters $rDisp$, $rForce$, $Uforce$.

$$\begin{aligned}
 rDisp &= 1.11 + 27.8\rho_v - 0.5e^v + 0.14 \ln\left(\frac{s\sqrt{f_y}}{31.62D_l}\right) - 1.12\left(\frac{f_y}{1000}\right) \\
 rForce &= -0.67 + 0.43\left(\frac{s}{d}\right) + 14.52\rho_l + 41.09\rho_v + 0.75\left(\frac{f_y}{1000}\right) \\
 uForce &= -0.8 + 23.23\rho_v - 8.38\left(\frac{A_v f_{yv}}{A_g f'_c}\right) + 1.96\left(\frac{f_{yv}}{1000}\right)
 \end{aligned} \tag{1}$$

where ρ_l, ρ_v are the ratio of longitudinal and transverse steel; $v = P/A_g f'_c$ is the ALR; s is the spacing of transverse reinforcement; d is the effective depth.

Through statistical data, Lee et al. [12] proposed the simplified equation to estimate the parameters that controlled the backbone curve, such as M_{cr} , M_y , M_c , k_{cr} , k_{y0} , k_{c0} , k_{n0} as presented in Figure 6.

$$\begin{aligned}
 M_{cr} &= e^{-2.94} b^{0.75} h^{1.52} L^{0.34} \rho_l^{0.21} \rho_v^{0.05} \\
 M_y &= e^{-0.95} b^{0.93} h^{1.23} L^{0.49} \rho_l^{0.54} \rho_v^{0.14} \\
 M_c &= e^{-2.45} b^{0.81} h^{1.25} L^{0.45} \rho_l^{0.51} \rho_v^{0.07} \\
 k_{cr} &= e^{1.33} b^{1.01} h^{1.86} (v + 0.1)^{0.58} \rho_v^{-0.19} \left(\frac{a}{d}\right)^{-0.26} \left(\frac{\tau}{31.62\sqrt{f'_c}}\right)^{0.2} \\
 k_{y0} &= e^{0.4} b^{0.99} h^{1.87} (v + 0.1)^{0.64} \rho_v^{-0.23} \left(\frac{a}{d}\right)^{-0.32} \left(\frac{\tau}{31.62\sqrt{f'_c}}\right)^{0.09}
 \end{aligned} \tag{2}$$

$$\tag{3}$$

$$k_{c0} = e^{-4.6} b^{0.94} h^{2.4} (\nu + 0.1)^{0.97} \rho_v^{-0.05} \left(\frac{a}{d}\right)^{-0.6} \left(\frac{\tau}{31.62\sqrt{f'_c}}\right)^{0.64}$$

$$k_{n0} = e^{-1.04} b^{0.74} h^{1.94} (\nu + 0.1)^{0.69} \rho_v^{-0.26} \left(\frac{a}{d}\right)^{-0.3} \left(\frac{\tau}{31.62\sqrt{f'_c}}\right)^{0.17}$$

where all parameters are in mm, MPa unit; L is the length of the equivalent cantilever column; a

is the shear span; $\tau = V_n/bh$ is the nominal shear stress (MPa); $\nu = P/A_g f'_c$ is the ALR.

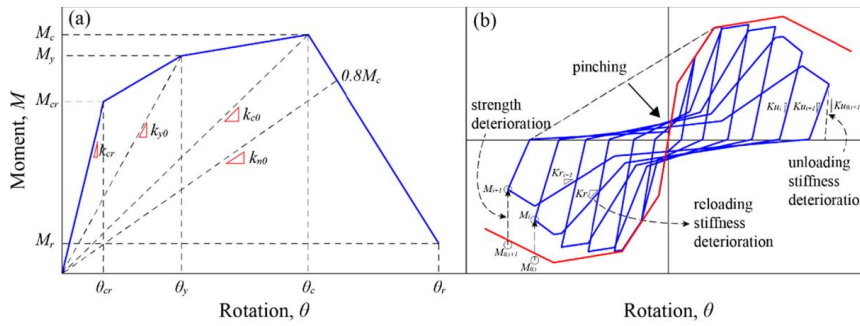


Figure 6. Backbone and cyclic curves for the Pinching4 model (Lee et al. [12])

2. Research methodology

The hysteresis loops of RC rectangular columns were implemented by OpenSees through four cases as follows:

Case 1: using the force-based beam-column element,

Case 2: using the displacement-based beam-column element;

Case 3: using the plastic hinge element;

Case 4: using three-spring model (shear, slip, and axial springs).

A thorough comparison of the results from these four cases was conducted against experimental test results, leading to insightful

discussions. This multifaceted approach not only provided a nuanced understanding of the structural response but also facilitated a comprehensive assessment of the simulation outcomes in relation to real-world observations.

2.1. Using force-based beam-column element

The force-based beam-column element is used to build a force-beam-column element object based on the iterative force-based formulation. In force-based beam-column element, some numerical integration options could be used to determine and encompass both distributed plasticity and plastic hinge integration. The command of the forced-based beam-column element is as follows:

$$\text{element forceBeamColumn } \$eleTag \ \$iNode \ \$jNode \ \$transfTag \ "IntegrationType \ arg1 \ arg2 \ ..." \ < -mass \ \$massDens \ > \ < -iter \ \$maxIters \ \$tol \ > \quad (4)$$

where $\$eleTag$ is the element tag; $\$iNode \ \$jNode$ is the end nodes I and J; $\$transfTag$ is the identifier for previously-defined coordinate-transformation object; $IntegrationType \ arg1 \ arg2 \dots$ specify weights and locations of integration points and their associated section force-deformation

models; $\$massDens$ is the element mass density per unit length (optional, default=0.0); $\$maxIters$ is the maximum number of iterations to undertake to satisfy element compatibility (optional, default=10); $\$tol$ is the tolerance for satisfaction of element compatibility (optional, default=10-12).

The displacement-based beam-column element is used to conduct a displacement-beam-column element object based on the displacement formulation considering the spread

$$\begin{aligned} & \textit{element dispBeamColumn } \$eleTag \ \$iNode \ \$jNode \ \$numIntgrPts \ \textit{sections} \\ & \$secTag1 \ \$secTag2 \ \dots \ \$transfTag \ - \ \textit{mass} \ \$massDens \ - \ \textit{cMass} > \\ & < \ - \ \textit{integration} \ \$intType > \end{aligned} \quad (5)$$

where $\$numIntgrPts$ is the number of integration points along the element; $\$secTag$ is the section tag of the element; $\$secTag1 \ \$secTag2 \ \dots$ are section object tags; $\$transfTag$ is the identifier for coordinate-transformation; $\$massDens$ is the element mass density per unit length (optional, default = 0.0); $-\textit{cMass}$ expresses to form consistent mass matrix (optional, default = *lumped mass matrix*); $\$intType$ is the numerical integration type (there are some options such as Lobotto, Legendre, Radau, NewtonCotes, Trapezoidal, default = *Legendre*);

2.2. Using plastic hinge element

$$\begin{aligned} & \textit{element forceBeamColumn } \$eleTag \ \$iNode \ \$jNode \ \$transfTag \ \textit{"HingeRadau } \$sec1 \\ & \$LpI \ \$secTagJ \ \$LpJ \ \$secTagInterior" < \ - \ \textit{mass} \ \$massDens \\ & > \ - \ \textit{iter} \ \$maxIters \ \$tol > \end{aligned} \quad (6)$$

where $\$secTagI$ is section tag of node I; $\$LpI$ is the PHL at end I; $\$secTagJ$ is the section tag of node J; $\$LpJ$ is the PHL at end J; $\$secTagInterior$ is the section object on the element interior; $\$transfTag$ is the coordinate-transformation tag; $\$maxIters$ is the maximum number of iterations (optional, default=1); $\$tol$ is the calculation tolerance for satisfying element compatibility (optional, default=10-16);

The PHL parameters ($\$LpI, \LpJ) are gotten from the PHL calculation in the previous section. The simulated results are presented in Table 4.

Pinching4 material:

of plasticity along the element. The OpenSees command of the displacement-based beam-column element is as follows:

Based on Scott et al. [13,14] and the PHLs that are calculated in the previous section, the beam-column element with PHL was used to simulate the columns through the OpenSees platform. The plastic hinge element command is used to build a force-beam-column element object based on the non-iterative (or iterative) flexibility formulation. The locations and weights of the integration points are derived from plastic hinge integration, allowing the users to assign PHLs at the ends of elements. The Gauss integration with two points is applied for the element interior while the Gauss-Radau integration is used over lengths of $4LpI$ and $4LpJ$ at the ends of elements. The OpenSees command is as follows:

The pinching effect is known as the tendency of the stiffness degradation when the element is unloaded. The loss of the stiffness at the neutral position results in low energy dissipation. The pinching effect is related to crack closure, shear lock, and slippage of longitudinal reinforcing.

Pinching parameters: the pinching behavior is simulated by three parameters, i.e., $rDisp$, $rForce$, $uForce$. While $rDisp, rForce$ control the pinching behavior of reloading and unloading branch, $uForce$ controls of the degree of pinching. Based on the previous experimental data, Lee et al. [12] proposed the algebraic equation to determine $rDisp, rForce, uForce$, and damage index δ_i as presented in Eqs. (7-10)

$$rDisp = 1.11 + 27.8\rho_v - 0.5e^r + 0.14 \ln\left(\frac{s\sqrt{f_y}}{31.62d_b}\right) - 1.12\left(\frac{f_y}{1000}\right); r = \frac{P}{A_g f'_c} \quad (7)$$

$$rForce = -0.67 + 0.43\left(\frac{S}{d}\right) + 14.52\rho_l + 41.09\rho_v + 0.75\left(\frac{f_y}{100}\right) \quad (8)$$

$$uForce = 0.8 + 23.23\rho_v - 8.38\left(\frac{A_v f_{yv}}{A_g f'_c}\right) + 1.96\left(\frac{f_{yv}}{1000}\right) \quad (9)$$

Damage index δ_i was presented in Eq. (7)

$$\delta_i = \delta_{disp} + \delta_{erg} = \alpha_1 \left(\frac{d_{max,i}}{d_f}\right)^{\alpha_3} + \alpha_2 \left(\frac{\sum E_i}{E_t}\right)^{\alpha_4} \quad (10)$$

where $d_{max,i}$ is the maximum deformation demand of loading cycle i^{th} ; d_f is the deformation at failure stage; E_i is the energy dissipation at loading cycle i ; E_t is the capacity of energy dissipation up to the yield point in the monotonic backbone curve. Four parameters ($\alpha_1, \alpha_2, \alpha_3$ and α_4) should be used for

$$\delta_i = \alpha_2 \left(\frac{\sum E_i}{E_t}\right) \quad (11)$$

$$\alpha_2 = e^{-5.82} \left(\frac{A_s f_y}{A_v f_{yv}}\right)^{1.57} \left(\frac{V_s}{V_n}\right)^{1.15} \left(\frac{f_y}{1000}\right)^{-3.18} \quad (12)$$

where α_2 is the damaged coefficient; V_s is the shear strength of transverse reinforcement; V_n is the nominal shear strength;

The pinching4 parameters of tested columns were presented in Tables (3-4)

3. The proposed model for hysteresis loop

Based on the proposal of Lee et al. [12], the author proposed a new model for columns with three springs, i.e., shear, slip, and axial springs. To obtain the hysteresis loop, the tested columns can be simulated by the column element with a fix at two ends. The column element was simulated by a fiber section that can capture the flexure response. And, three springs, i.e., shear, bar slip, and axial springs were put at column ends as presented in Figure 9. The shear spring will capture the stiffness and shear degradation,

estimating the degree of cyclic deterioration in strength, unloading and reloading stiffness.

According to Lignos et al. [15], and Haselton et al. [16], it can simulate the cyclic deteriorations by using simplified equations Eqs. (8-9):

the slip spring will record the slip rotation, and the axial spring will transmit the axial compression force. The proposed model can capture the degradation of shear strength, and stiffness, and express the strain penetration of longitudinal bars, and axial compression load at failure. Some models also were conducted to compare with tested results by using OpenSees (force-based beam-column, displacement-based beam-column, and plastic hinge beam-column elements).

The columns were simulated by the fiber section analysis method using Concrete02 and Steel02 material. The Concrete02 material is used for both the confined and unconfined concrete. The confined concrete material is applied for the concrete core of columns, while the unconfined concrete material is assigned for

the concrete cover of columns. In addition, the Steel02 material is assigned for longitudinal steel.

$$\text{uniaxialMaterial Concrete02 } \$IDconcCore \$f_{c1} \$eps_1 \$f_{c2} \$eps_2 \$lambda \$f_{tc} \$E_{ts} \quad (13)$$

where $\$IDconcCore$ is the material ID tag; $\$f_{c1}$ is the maximum compressive stress of concrete; $\$eps_1$ is the strain at maximum stress; $\$f_{c2}$ is the ultimate compressive stress of concrete; $\$eps_2$ is the strain at ultimate stress; $\$lambda$ is the ratio between unloading slope at

The Concrete02 material command in OpenSees is as follows:

$\$eps_2$ and initial slope (E_c); $\$f_{tc}$ is the maximum tensile stress of concrete; $\$E_{ts}$ is the tension softening stiffness;

Similarly, the Steel02 material command in OpenSees is as follows:

$$\text{uniaxialMaterial Steel02 } \$IDreinf \$f_y \$E_s \$Bs \$R0 \$cR1 \$cR2 \quad (14)$$

where $\$IDreinf$ is the material ID tag; $\$f_y$ is the yield stress of steel; $\$E_s$ is the modulus of steel; $\$Bs$ is the strain hardening ratio; $\$R0, \$cR1, \$cR2$ is the parameters that control the transition from elastic to plastic branches;

BondSP01 material: this material model is used to conduct a uniaxial material object

$$\text{uniaxialMaterial BondSP01 } \$matTag \$F_y \$S_y \$F_u \$S_u \$b \$R \quad (15)$$

where $\$matTag$ is the material tag; $\$F_y$ is the yield strength of reinforcing steel; $\$S_y$ is the rebar-slip at member interface under yield stress; $\$F_u$ is the ultimate strength of the reinforcement steel; $\$S_u$ is the rebar-slip at the loaded ends at the fracture strength; $\$b$ is the initial hardening ratio in the monotonic slip versus bar stress response (taken as 0.3~0.5); $\$R$ is the pinching factor for the cyclic slip versus bar response (taken as 0.5~1.0);

$$\begin{aligned} &\text{uniaxialMaterial Pinching4 } \$matTag \$ePf1 \$ePd1 \$ePf2 \$ePd2 \$ePf3 \\ &\$ePd3 \$ePf4 \$ePd4 < \$eNf1 \$eNd1 \$eNf2 \$eNd2 \$eNf3 \$eNd3 \$eNf4 \\ &\$eN > \$rDispP \$rForceP \$uForceP < \$rDispN \$rForceN \$uForceN \\ &> \$gK1 \$gK2 \$gK3 \$gK4 \$gKLim \$gD1 \$gD2 \$gD3 \$gD4 \$gDLim \\ &\$gF1 \$gF2 \$gF3 \$gF \end{aligned} \quad (16)$$

where $\$matTag$ is the integer tag identifying material; $\$ePf1 \$ePf2 \$ePf3 \$ePf4$ are the floating point values defining force points on the positive response envelope;

considering strain penetration effects at the column-to-base interface. In this model, the bond-slip related with strain penetration will typically occur along a part of anchorage length. The OpenSees command is as follow:

Pinching4 material: is used to construct a uniaxial material that represents a 'pinched' load-deformation response and exhibits degradation under cyclic loading. Cyclic degradation of strength and stiffness occurs in three ways: unloading stiffness degradation, reloading stiffness degradation, strength degradation.

$\$ePd1 \$ePd2 \$ePd3 \$ePd4$ are the floating point values defining deformation points on the positive response envelope; $\$eNf1 \$eNf2 \$eNf3 \$eNf4$ are the floating

point values defining force points on the negative response envelope; $\$eNd1$ $\$eNd2$ $\$eNd3$ $\$eNd4$ are the floating point values defining deformation points on the negative response envelope; $\$rDispP$ is the floating point value defining the ratio of the deformation at which reloading occurs to the maximum historic deformation demand; $\$fFoceP$ is the floating point value defining the ratio of the force at which reloading begins to force corresponding to the maximum historic deformation demand; $\$uForceP$ is the floating point value defining the ratio of strength developed upon unloading from negative load to the maximum strength developed under monotonic loading; $\$rDispN$ is the floating point value defining the ratio of the deformation at which reloading occurs to the minimum historic deformation demand; $\$fFoceN$ floating point value defining the ratio of the force at which reloading begins to force corresponding to the minimum historic deformation demand; $\$uForceN$ is the floating point value defining the ratio of strength developed upon unloading from negative load to the minimum

strength developed under monotonic loading; $\$gK1$ $\$gK2$ $\$gK3$ $\$gK4$ $\$gKLim$ are the floating point values controlling cyclic degradation model for unloading stiffness degradation; $\$gD1$ $\$gD2$ $\$gD3$ $\$gD4$ $\$gDLim$ are the floating point values controlling cyclic degradation model for reloading stiffness degradation; $\$gF1$ $\$gF2$ $\$gF3$ $\$gF4$ $\$gFLim$ are the floating point values controlling cyclic degradation model for strength degradation; $\$gE$ is the floating point value used to define maximum energy dissipation under cyclic loading. Total energy dissipation capacity is defined as this factor multiplied by the energy dissipated under monotonic loading; $\$dmgType$ is the string to indicate type of damage (option: “cycle”, “energy”).

Axial-spring: accounts for the transmission effect of axial compression load. Axial-spring is used to construct an axial limit curve object that is used to define the point of axial failure for a *LimitStateMaterial* object. The *OpenSees* command is as below:

$$\begin{aligned} & \text{limitCurve Axial } \$curveTag \$eleTag \$Fsw \$Kdeg \$Fres \$defType \\ & \$forType < \$ndI \$ndJ \$dof \$perpDirn \$delta > \end{aligned} \quad (17)$$

where $\$curveTag$ is the unique *LimitCurve* tag; $\$eleTag$ is the integer element tag for the associated beam-column element; $\$F_{sw}$ is the floating point value describing the amount of transverse reinforcement; $\$Kdeg$ is the floating point value for the slope of the third branch in the post-failure backbone, assumed to be negative; $\$Fres$ is the floating point value for the residual force capacity of the post-failure backbone; $\$defType$ is the integer flag for type of deformation defining the abscissa of the limit curve (1 = maximum beam-column chord rotations; 2 = drift based on displacement of nodes ndI and ndJ); $\$forType$ is the integer flag for type of force defining the

ordinate of the limit curve (0 = force in associated limit state material; 1 = shear in beam-column element; 2 = axial load in beam-column element); $\$ndI$ is the integer node tag for the first associated node (normally node I of $\$eleTag$ beam-column element); $\$ndJ$ is the integer node tag for the second associated node (normally node J of $\$eleTag$ beam-column element); $\$dof$ is the nodal degree of freedom to monitor for drift. $\$perpDirn$ is the perpendicular global direction from which length is determined to compute drift. $\$delta$ is the drift (floating point value) used to shift axial limit curve.

This proposed model was verified by tested results of Pham and Hung [17] and Hung et al. [18] as presented in Tables (1-4). The results revealed that:

The displacement-based beam-columns element more exactly the shear strength and drift ratio at peak strength to compare with force-based beam-column and plastic hinge elements.

The accuracy of the solution in the OpenSees platform could be improved by increasing the element number or integration points. It could be implemented by either increasing the integration point number or the element number for the

force-based beam-column element or only increasing the number of elements for the displacement-based beam-column element. In the case of force-based beam-column elements, both local and global quantities will converge fast if increasing the number of integration points. In the case of displacement-based beam-column elements, higher derivatives converge slower to the exact solution. Therefore, the exact determination of local response quantities (such as curvatures) requires a finer finite element mesh than the accurate determination of global response quantities (such as rotations).

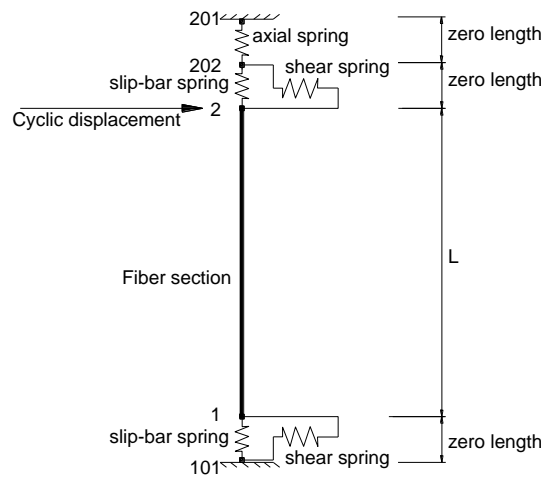


Figure 7. Column model

Three simulation elements, i.e., forced-based beam-column, displacement-based beam-column, and plastic hinge elements, could not exactly simulate the behavior RC rectangular columns both peak strength and drift at peak strength. Also, they could not capture the degradation of strength and stiffness of columns.

Using a 3-spring (shear, axial, and slip springs) model can simulate perfectly the strength and stiffness degradation. The simulation results are reasonable with the average ratio of 0.982 and 1.039 for peak strength and drift at peak strength.

4. Conclusions

Based on Lee et al.'s model [12], the author proposed a novel model with 3 springs to

simulate the hysteresis loops of RC columns. Some conclusions are presented below:

It could not precisely simulate the response of columns if only using force-beam column, displacement beam-column, or plastic hinge elements. Besides, it could not capture the degradation of shear strength and stiffness. However, force-beam column and plastic hinge elements could give a reasonable result for the peak strength.

The separate use of the forced-based beam-column, displacement-based beam-column, or plastic hinge element cannot simulate accurately the hysteresis loops.

A three-spring model with shear, slip, and axial springs was proposed to simulate the

hysteresis loop of tested columns through the Opensees platform with good accuracy. The simulation results can capture the column behavior, i.e., peak strength, drift at peak strength, shear strength, and stiffness degradation, pinching behavior.

However, it's necessary to note that while this model shows promising results for normal RC

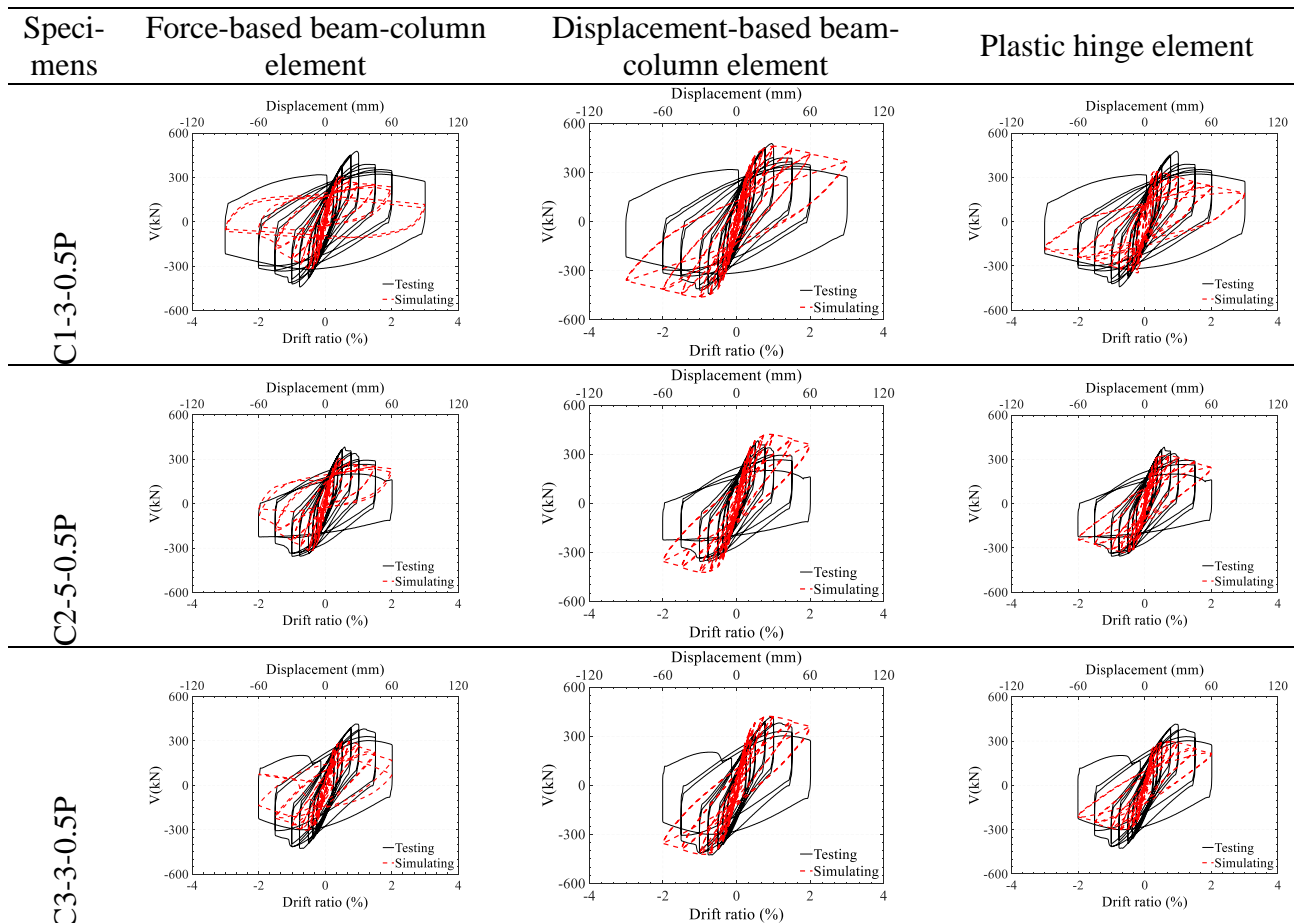
columns, it may not be suitable for slender RC columns with medium to high slenderness ratios. This suggests a need for further research and development of a new model that can accurately simulate the hysteresis loops of slender RC columns, taking into account their unique characteristics and challenges.

Table 1. Pinching4 parameters

Specimens	$rDisp$	$rForce$	$uForce$	α_2	V_{cr} (kN)	DR_{cr}	V_y (kN)	DR_y	V_{max} (kN)	DR_{max}	V_u (kN)	DR_u
C1-3-0.5P	0.276	0.647	0.194	0.363	52	0.01%	388	0.05%	517	1.50%	439	3.00%
C2-5-0.5P	0.276	0.647	0.194	0.363	41	0.01%	305	0.10%	407	0.30%	346	2.00%
C3-3-0.5P	0.188	0.517	0.120	0.317	46	0.01%	344	0.05%	458	0.25%	389	2.00%
C3-3-0.1P	0.460	0.517	0.131	0.332	38	0.01%	284	0.50%	379	1.20%	322	7.00%

Note: V_{max}, DR_{max} is taken by the peak load and drift ratio at peak load of tested result; V_y, DR_y are taken by the load and drift ratio at $V_y = 0.75V_{max}$; V_{cr}, DR_{cr} is calculated by Eqs. (2-5); V_u, DR_u are the load and drift ratio at $V_u = 0.85V_{max}$;

Table 2. Simulation results



C3-3-0.1P

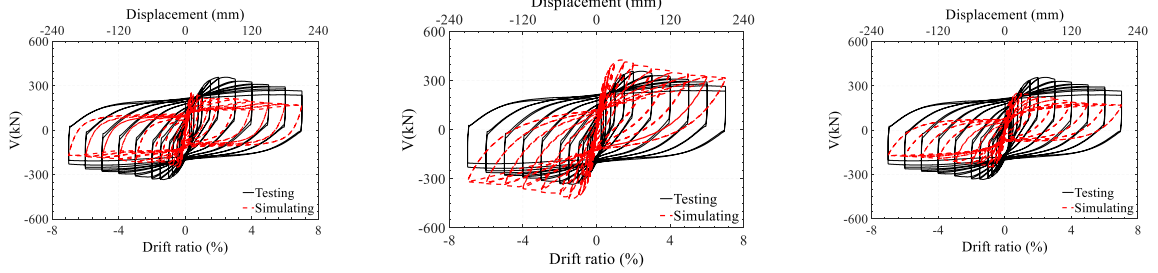


Table 3. Simulation results using 3 springs

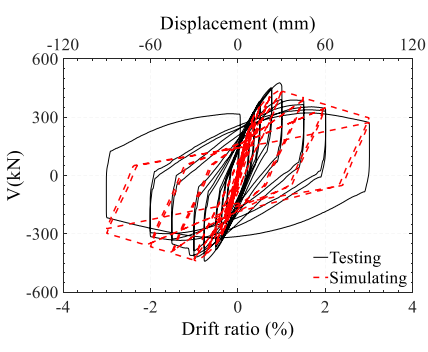
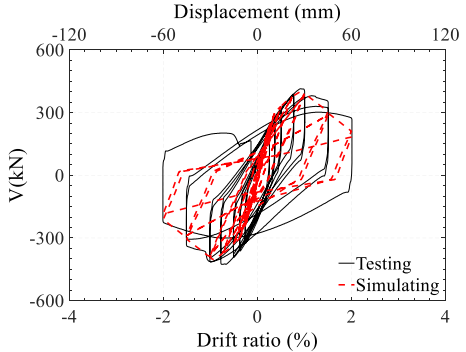
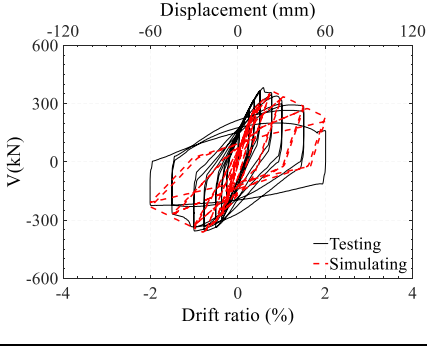
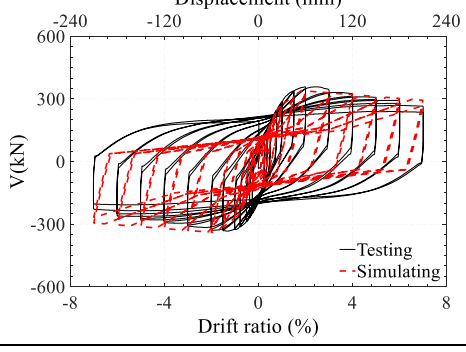
Specimens	3-spring model	
C1-3-0.5P		
C2-5-0.5P		

Table 4. Summary of OpenSees model results

Columns	Force based beam-column element		Displacement based beam-column element		Plastic hinge element		Three-spring model	
	$\frac{V_{sim}}{V_{test}}$	$\frac{DR_{sim}}{DR_{test}}$	$\frac{V_{sim}}{V_{test}}$	$\frac{DR_{sim}}{DR_{test}}$	$\frac{V_{sim}}{V_{test}}$	$\frac{DR_{sim}}{DR_{test}}$	$\frac{V_{sim}}{V_{test}}$	$\frac{DR_{sim}}{DR_{test}}$
C1-3-0.5P	0.687	0.573	1.011	1.181	0.751	0.323	0.958	1.141
C2-5-0.5P	0.871	0.654	1.171	1.212	0.91	0.831	1.006	1.093
C3-3-0.5P	0.719	0.682	1.012	1.034	0.716	0.86	0.967	1.095
C3-3-0.1P	0.742	0.185	1.245	0.633	0.732	0.331	0.996	0.827
Average	0.755	0.524	1.110	1.015	0.777	0.586	0.982	1.039
COV	0.107	0.440	0.106	0.262	0.115	0.511	0.023	0.138

References

- [1] Huy, P.P.A., Yuen, T.Y., Hung, C.C., Mosalam, K.M. (2022). Seismic behaviour of full-scale lightly reinforced concrete columns under high axial loads. *Journal of Building engineering* (56), 104817. <https://doi.org/10.1016/j.job.2022.104817>.
- [2] Pham, P.A.H. (2022). Shear strength model of large-scale reinforced concrete rectangular columns with light transverse reinforcement. *Asian journal of Civil engineering* (24), 219-244. <https://doi.org/10.1007/s42107-022-00499-9>.
- [3] Huy, P.P., Ben L.M., Đai, P.B. (2023). Nghiên cứu các yếu tố ảnh hưởng đến khả năng chịu cắt của cột bê tông cốt thép có xét đến ảnh hưởng của lực nén. *Tạp chí Khoa học và Công nghệ Đại học Duy Tân* 4(59), 19–28.
- [4] Huy, P.P.A. (2023). Xây dựng đường bao khả năng chịu lực cho cột bê tông cốt thép có tiết diện chữ nhật. *Tạp chí Khoa học và Công nghệ - Đại học Đà Nẵng* 21(7), 63-68.
- [5] Huy, P.P.A., Long, Đ.H. (2016). Đánh giá ảnh hưởng của hàm lượng cốt dọc đến khả năng chịu cắt của dầm bê tông cốt thép theo lý thuyết miền nén cải tiến đơn giản. *Tạp chí Khoa học và Công nghệ - Đại học Đà Nẵng* 3(100), 68-74.
- [6] Clough, R.W. (1996). Effect of stiffness degradation on earthquake ductility requirements. *Second Japan Earthquake Engineering Symposium* (1), 227–32.
- [7] Takeda, T., Sozen, M.A., Nielsen, N.N. (1970). Reinforced concrete response to simulated earthquakes. *Journal of the structural division* (96), 2557–2573. <https://doi.org/10.1061/JSDEAG.0002765>.
- [8] Saatcioglu, M., Ozcebe, G. (1989). Hysteretic shear model for reinforced concrete members. *Journal of Structural engineering* (115), 132–148. [https://doi.org/10.1061/\(ASCE\)0733-9445\(1989\)115:1\(132\)](https://doi.org/10.1061/(ASCE)0733-9445(1989)115:1(132)).
- [9] Lowes, L.N., Altoontash, A. (2003). Modeling reinforced-concrete beam-column joints subjected to cyclic loading. *Journal of Structural engineering* (129), 1686–97. [https://doi.org/10.1061/\(ASCE\)0733-9445\(2003\)129:12\(1686\)](https://doi.org/10.1061/(ASCE)0733-9445(2003)129:12(1686)).
- [10] Sezen, H., Chowdhury, T. (2009). Hysteretic model for reinforced concrete columns including the effect of shear and axial load failure. *Journal of Structural engineering* (135), 139–46. [https://doi.org/10.1061/\(ASCE\)0733-9445\(2009\)135:2\(139\)](https://doi.org/10.1061/(ASCE)0733-9445(2009)135:2(139)).
- [11] Lignos, D., Krawinkler, H. (2011). Deterioration modeling of steel components in support of collapse prediction of steel moment frames under earthquake loading. *Journal of Structural engineering* (137), 1291–1299. [https://doi.org/10.1061/\(ASCE\)ST.1943-541X.0000376](https://doi.org/10.1061/(ASCE)ST.1943-541X.0000376).
- [12] Lee, C.S., Han, S.W. (2018). Computationally effective and accurate simulation of cyclic behaviour of old reinforced concrete columns. *Journal of Engineering structures* (173), 892–907. <https://doi.org/10.1016/j.engstruct.2018.07.020>.
- [13] Scott, M.H., Fenves, G.L. (2006). Plastic hinge integration methods for force-based beam-column elements. *Journal of Structural engineering* (132), 244–252. [https://doi.org/10.1061/\(ASCE\)0733-9445\(2006\)132:2\(244\)](https://doi.org/10.1061/(ASCE)0733-9445(2006)132:2(244)).
- [14] Scott, M.H., Ryan, K.L. (2013). Moment-Rotation Behavior of Force-Based Plastic Hinge Elements. *Journal of Earthquake spectra* (29), 597–607. <https://doi.org/10.1193/1.4000136>.
- [15] Lignos, D.G., Krawinkler, H. (2011). Deterioration modeling of steel components in support of collapse prediction of steel moment frames under earthquake loading. *Journal of Structural Engineering* (137), 291–302. [https://doi.org/10.1061/\(ASCE\)ST.1943-541X.0000376](https://doi.org/10.1061/(ASCE)ST.1943-541X.0000376).
- [16] Haselton, C.B., Liel, A.B., Taylor-Lange, S.C., Deierlein, G.G. (2016). Calibration of model to simulate response of reinforced concrete beam-columns to collapse. *ACI structural Journal* (113), 1141-1152. <https://doi.org/10.14359/51689245>.
- [17] Pham, P.A.H., Hung, C.C. (2023). Assessment of plastic hinge length in reinforced concrete columns. *Journal of Structure and Infrastructure Engineering* (12) ,1–16. <https://doi.org/10.1080/15732479.2023.2263432>.
- [18] Hung, C.C., Pham, P.A.H., Yuen, T.Y., Mosalam, K.M. (2024). Full-scale cyclic testing of slender RC columns bent in double curvature under high axial load. *Journal of Building engineering* (82), 108186. <https://doi.org/10.1016/j.job.2023.108186>.